

BROAD FREQUENCY VIBRATION ENERGY HARVESTING CONTROL APPROACH BASED ON THE MAXIMUM POWER TRANSFER THEOREM

Alexander V. Pedchenko

Mechanical Engineering
Vanderbilt University
Nashville, TN 37235

alexander.v.pedchenko@vanderbilt.edu

Eric J. Barth

Mechanical Engineering
Vanderbilt University
Nashville, TN 37235

eric.j.barth@vanderbilt.edu

ABSTRACT

A control law for an electromagnetic vibration energy harvester is derived using the maximum power transfer theorem. Using regenerative electronics, the controller cancels the reactive portion of the harvester's impedance by eliminating the effect of mechanical inertia and stiffness elements, and the coil's electrical inductive element. The result is an energy harvester approach that captures more vibrational energy than a passive tuned harvester. It is shown that the controlled system acts like an infinite series of passive harvesters tuned to all frequency components within a certain frequency range. The control approach also avoids the delay and computational overhead of a Fast Fourier Transform as it does not require the explicit calculation of the excitation frequency. An experimental prototype harvester was built and characterized. The prototype's multi-domain dynamics were modeled using bond-graph techniques, and its behavior as a passive harvester was experimentally validated. The prototype's behavior under the proposed control method is simulated and compared to the passive case. It is shown that the proposed control method harvests more power for a range of excitation frequencies than the passive harvester.

NOMENCLATURE

b	Equivalent linear viscous damping of the harvester when leads are open [N/(m/s)]
C	General capacitive component in bond graph model
GY	General gyrator component in bond graph model
I	General inertial component in bond graph model
I	Current running through coil winding [A]
j	$\sqrt{-1}$
k	Equivalent linear stiffness of the harvester [N/m]

K_f	Motor force constant/back emf constant [N/A]/[V/(m/s)]
L_{LVC}	Inductance of the LVC [H]
m	Equivalent mass of the harvester's proof mass [kg]
P	Harvester center of mass position relative to bridge position [m]
R	General resistive component in bond graph model
R_{LVC}	Resistance of the LVC [Ohms]
S_e	General effort source component in bond graph model
U	Force exerted by the harvester during active control [N]
V_{thev}	Thevenin equivalent voltage source [V]
X	Absolute bridge position measured from static equilibrium [m]
Y	Absolute harvester center of mass position measured from static equilibrium [m]
Z	General impedance component in bond graph model
Z_{source}	Thevenin equivalent internal impedance of the harvester
Z_{load}	Load impedance
ω	Operational frequency [rads/s]
ω_n	Natural frequency [rads/s]

INTRODUCTION

Currently, bridges in the U.S. are visually inspected biennially [1]. When this fact is coupled with the U.S. Department of Transportation claim that 25% of bridges are "functionally obsolete" or "structurally deficient", it becomes clear that more rigorous structural monitoring is required [2]. This need was made further apparent by the tragic 2007 collapse of I-35W Mississippi River Bridge in Minneapolis. An official report on the

status of the bridge in March 2001, mentioned some poor fatigue details of the bridge, but not to the degree of needing to close the bridge to traffic for repairs. However, the report did recommend how the placement of strain gauges at several key locations coupled with detailed analysis could help predict the bridge's behavior in the future. The report went as far as recommending similarly instrumenting other bridges [3]. This recommendation was fully taken into account with the construction of the new I-35W Saint Anthony Falls Bridge, the replacement for its collapsed predecessor, which boasts 323 structural monitoring sensors [4]. These sensors can be used to assess the bridge's condition by providing metrics such as deck movements, stresses, and temperatures.

While the Saint Anthony Falls Bridge, costing \$234 million, is an impressive feat in structural monitoring, it would be impossible to retrofit all existing bridges with such an extensive sensor array. However, key placement of strain gauges, accelerometers, and/or acoustic sensors, transmitting continuously, or even at regular and relatively short intervals, would improve the current state of structural monitoring.

Whichever sensor type is chosen for observing structural integrity, data acquisition and transfer require some sort of power source. While new bridges, such as Saint Anthony Falls, could include sensor instrumentation during the construction process, adding wired networks of sensors, power and data acquisition/processing is difficult and expensive [5]. Thus, ideally, wireless sensors and power sources will be used.

The research associated with this paper is concerned with developing a wireless, self-contained power sources for said wireless sensors. The power source candidates considered were under the constraints of being ideally self-contained, robust, and requiring little to no maintenance during the lifetime of the bridge. This eliminates batteries as a viable candidate due to the need of their replacement on a regular basis. Thus, solar-based, wind-based, and energy harvesting relying on the vehicle traffic on the bridge were considered. Sun and wind power were avoided, as both are not guaranteed to be present when they are needed most (i.e., heavy traffic conditions do not necessarily occur on sunny or windy days), while their use also limits mounting options for the sensors (as it is usually desirable to keep lines between a sensor and its power supply at a minimum length).

Bridge traffic provides a convenient source of mechanical power which can be harvested in several ways. The three most prevalent forms of electromechanical conversion/energy harvesting are electrostatic, piezoelectric, and electromagnetic. Due to its robustness, life span, and relative ease of controllability, electromagnetic harvesting was chosen as the power harvesting mechanism. An in-depth justification for this choice can be found in [6].

The inherent weakness of conventional vibrational electromagnetic energy harvesters (VEH's) is that they rely on an

input mechanical excitation of a single pre-determined frequency - the generator's resonant frequency [7]. However, it is known that not only do different bridges oscillate at different frequencies [1], requiring a specific generator for a particular bridge, but any one bridge will also oscillate differently depending on traffic conditions [8]. Furthermore, often the movement of any particular point on a bridge will contain multiple frequency components [9].

This manuscript presents a method aimed at addressing the shortcomings of a conventional VEH through the use of active control. The proposed methodology relies on actively altering the vibrational response of the harvester in order to maximize the net energy captured. The motion is altered in a specific fashion in accordance to a control law derived from the harvester's model and the maximum power transfer theorem.

METHODOLOGY AND RESULTS

Controller Purpose

The proposed technique for energy harvesting can be roughly summarized as a method of creating a broad resonance frequency range for a VEH. An electromagnetic energy harvester's dynamics are essentially similar to those of a conventional mass-spring-damper system exposed to oscillatory excitation. A given mass-spring-damper system passively reacts to its excitation source, having a single resonant frequency at which the amplitude of the oscillation of the mass relative to the amplitude of the oscillation of the excitation source is the greatest.

The proposed control scheme, in contrast, alters the passive response of the system to behave as if the excitation seen by the mass-spring-damper is at the system's resonant frequency. Since this holds true for any frequency component in the excitation, the resulting response is equivalent to an infinite series of harvesters tuned to span a range of resonant frequencies. Since a conventional vibrational electromagnetic energy harvester relies on being excited by one particular frequency to generate appreciable power (energy capture rate falls off rapidly when the excitation frequency is even slightly different from the VEH's resonant frequency), it can only be implemented in situation where a single known frequency will be present. The proposed controller uses a VEH as an electromagnetic generator as well as a linear motor, thereby allowing a range of excitation frequencies to elicit resonant-like behavior. This results in more energy being harvested.

Passive Electromagnetic Vibration Energy Harvesting

Figure 1 depicts a lumped parameter representation of a typical VEH attached to an excitation source, which, in our case, is a vibrating span of a bridge. In the figure, X represents the span's displacement in meters normal to the road surface and measured from its static equilibrium (when there's no traffic on the bridge), m represents the effective mass in kg of the proof mass of the VEH, b represents the harvester's mechanical viscous damping in N/(m/s), $k/2$ represents the stiffness value (in N/m) of

each of the two springs responsible for keeping the mass in a suspended and readily excited state, Y represents the absolute proof mass displacement in meters along the same direction as X , the “Linear mot/gen” represents the motor/generator effect on the harvester motion (which will be discussed later), and finally P represents the relative displacement between the proof mass and the bridge span (i.e., $P = X - Y$).

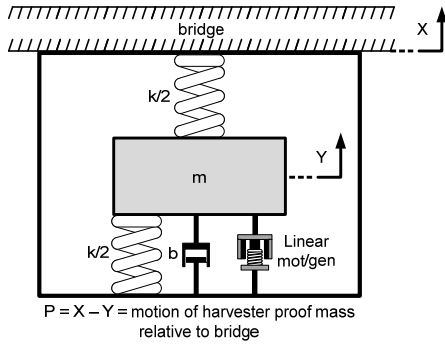


FIGURE 1. LUMPED PARAMETER REPRESENTATION OF ENERGY HARVESTER

Traffic passing over the bridge will elicit an oscillatory response in the span represented by the variable X . Conventionally, the form of X will be that of a group of sinusoids added together:

$$X(t) = A_1 \sin(\omega_1 t + \phi_1) + A_2 \sin(\omega_2 t + \phi_2) + \dots \quad (1)$$

where A_x represent the zero-to-peak amplitude [m] of the ω_x frequency [rads/s] component. As mentioned in the introduction, the existing frequency components’ amplitude and frequency values vary depending on a particular bridge, the position on a given bridge at which measurements are taken, and traffic conditions. Literature review showed oscillation varying from 0.25 mm to 1 mm in amplitude, and 3 to 9 Hz in frequency [8, 10, 11, 12, 13].

Williams et al. showed that a passive VEH harvests energy at a rate described by the following equation:

$$P_{avg} = \frac{m\zeta A^2 \left(\frac{\omega}{\omega_n}\right)^3 \omega^3}{\left[1 - \left(\frac{\omega}{\omega_n}\right)^2\right]^2 + \left[2\zeta \frac{\omega}{\omega_n}\right]^2} \quad (2)$$

where P_{avg} is the average power generated once the harvester reaches steady-state oscillations, m is the mass of the proof-mass of the harvester, ζ is the damping ratio between the system’s total parasitic damping (both mechanical and electrical) and the mechanical stiffness and inertia, ω_n is the harvester’s natural

frequency (i.e., $\sqrt{k/m}$, where k is the harvester’s equivalent stiffness), and A and ω are the amplitude and frequency at which the harvester is excited respectively. Figure 2 is a graphical representations of Eq. (2), where A , m , and ζ are held constant, while excitation frequency is varied from 3 to 12 Hz. The four curves represent passive harvesters having identical proof masses and damping ratios, but tuned to four different natural frequencies (4, 6, 8 and 10 Hz). The figure makes it easier to observe the large sensitivity passive harvesters have to the frequency at which they are excited.

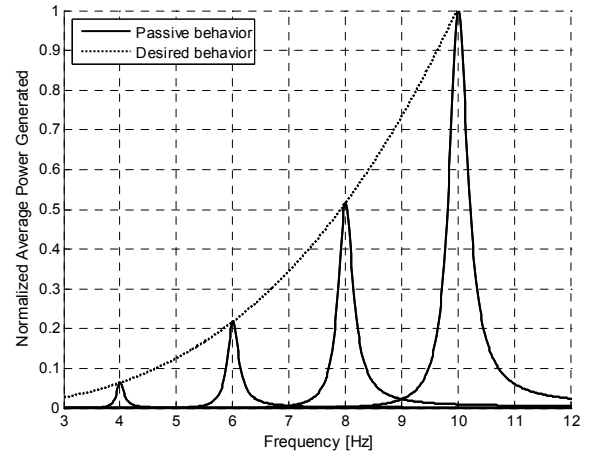


FIGURE 2. PASSIVE AND CONTROLLED BEHAVIOR

For any of the four passive VEHs, when excitation deviates by just a few hertz from the particular harvester’s natural frequency, power generation becomes insignificant. This prohibits the practical use of conventional VEHs on bridges, as the oscillatory behavior is not limited to a single known frequency. However, if a VEH could behave like a passive harvester excited at its natural frequency when excited by any single frequency or a combination of frequency components, it would harvest the maximum amount of energy theoretically possible. This type of desired behavior is shown by the dotted line in Fig. 2. This type of performance can be thought of as an infinite number of passive harvesters, the natural frequencies of which wholly define a certain frequency range of interest in which maximum electromagnetic energy capture occurs.

Description of Experimental Setup and Modeling

To achieve maximum power generation in the chosen frequency range of interest (3-12 Hz, largely based on what was seen in the literature) a physical setup was constructed and passive behavior was replicated and studied. The VEH manufactured for this purpose is shown in Fig. 3 and Fig. 4. It is comprised of a linear voice coil (LVC), a pair of compliant flexure mechanisms, an optical encoder, an accelerometer, and a super capacitor bank.

The LVC functions as a linear motor/generator, and provides the bulk of the proof mass. When functioning as a generator, the LVC's purpose is to harvest energy from the oscillatory excitation provided by the aluminum I-beam, to which it is rigidly attached, and to store the harvested energy in the super capacitor bank. The beam is rigidly attached to a medium-capacity LDS electromagnetic shaker, which simulates bridge vibrations. When functioning as a motor, the LVC will be required to use some of the energy in the super capacitor bank to enforce the desired behavior previously discussed, resulting in net positive power generation providing that the regenerative electronics are efficient.

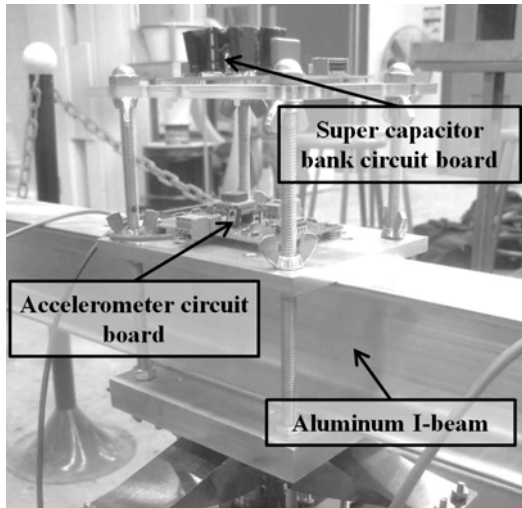


FIGURE 3. PHOTOGRAPH OF THE TOP PORTION OF THE VEH EXPERIMENTAL SETUP

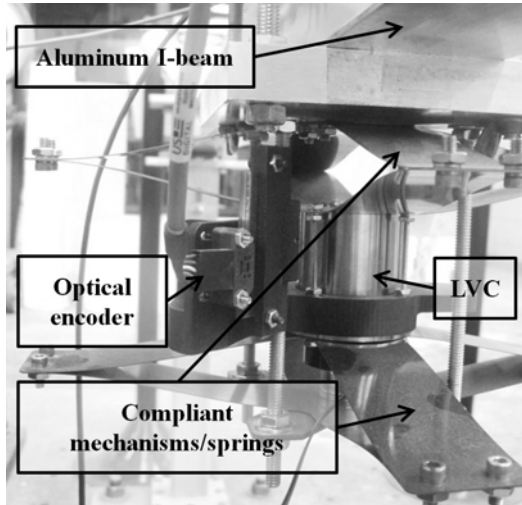


FIGURE 4. PHOTOGRAPH OF THE BOTTOM PORTION OF THE VEH EXPERIMENTAL SETUP

The compliant flexure mechanisms serve two purposes. They act as springs suspending the permanent magnet portion of the linear voice coil (i.e., proof mass), thereby allowing it to oscillate relative to the coil portion in response to an oscillatory excitation input. Their second purpose, and the reason the VEH design incorporates these custom made components instead of ordinary springs, is that they are very effective at restricting the motion between the coil and the permanent magnets of the LVC to their axis of alignment. The optical encoder and accelerometer sensors provide signals necessary for tracking the physical response of the VEH to its excitation and closing the control loop.

The dynamics of the VEH, shown in Figs. 3 and 4, can be described by a number of linear components interacting in the mechanical and electrical domains. Bond graph modeling methodology can be used to see this interaction in an intuitive way based on power flow.

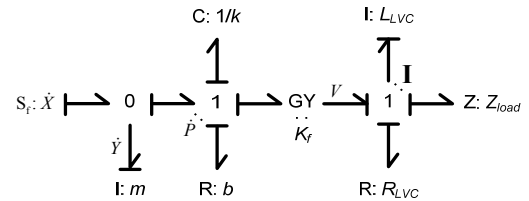


FIGURE 5. BOND GRAPH REPRESENTATION OF THE VEH

The bond graph depicts the power flow throughout the harvester experimental setup. A flow source $S_f = \dot{X}$ (velocity of the oscillations of the aluminum I-beam) perturbs the VEH's proof mass m . This perturbation is combined with the effects of the equivalent stiffness k (represented by the compliance $C = 1/k$) of the two compliant mechanisms/springs and the mechanical damping of the system b . The mass moves at the velocity \dot{Y} , while relative velocity seen by the equivalent stiffness and mechanical damping is \dot{P} (see Fig. 1). The same velocity \dot{P} is seen by the LVC (linear mot/gen component), which transforms it into a voltage V via a gyrator GY. The gyrator produces the voltage by scaling the velocity according to Eq. (3)

$$V = K_f \dot{P} \quad (3)$$

where K_f is the motor constant/back emf constant of the LVC. The generated voltage V causes a current I to flow through the LVC's winding.

Equation (4) shows the harvester's response to excitation X in terms of the absolute motion of its proof mass Y and the current running through the coil winding I

$$\sum F_{ext} = m\ddot{Y} = k(X - Y) + b(\dot{X} - \dot{Y}) + K_f I \quad (4)$$

By subtracting $m\ddot{Y}$ and adding $m\ddot{X}$ to both sides, Eq. (4) can be modified to be in terms of proof mass displacement relative to the bridge $P = X - Y$, which is not only a more intuitive metric of the proof mass motion, but also a quantity measured directly by the optical encoder shown in Fig. (4). This modified form is shown as Eq. (5).

$$\begin{aligned} m\ddot{X} &= m(\ddot{X} - \ddot{Y}) + b(\dot{X} - \dot{Y}) + k(X - Y) + K_f \mathbf{I} \\ m\ddot{X} &= m\ddot{P} + b\dot{P} + kP + K_f \mathbf{I} \end{aligned} \quad (5)$$

The second equation describing the VEH's behavior defines the relationship between the voltage developed due to the velocity of the LVC (Eq. (3)) relative to that of the bridge \dot{P} and the current running through the coil winding \mathbf{I} ; this relationship is shown as Eq. (6).

$$K_f \dot{P} - L_{LVC} \dot{\mathbf{I}} - R_{LVC} \mathbf{I} - Z_{load} \mathbf{I} = 0 \quad (6)$$

The voltage/current relationship is determined by the LVC's equivalent inductance L_{LVC} , its internal resistance R_{LVC} , and the electrical load connected across its leads Z_{load} . In a conventional VEH, Z_{load} behaves purely resistively. Its choice is not arbitrary and its derivation is discussed in the following section.

Derivation of the Ideal Load

An additional benefit of the bond graph model shown in Fig. 5, is the ease with which it is possible to cast the electromechanical system wholly into the mechanical or wholly into the electrical domain. Since the objective is to find which load, when attached across the VEH leads, will result in the maximum amount of power being transferred to it, the system should be cast into the electrical domain. Electrical power sources and their associated internal impedances are often analyzed using load matching techniques; tools for achieving maximum power transfer to the load, or achieving power transfer at maximum efficiency are readily available in the electrical domain. Additionally, when losses occur in both the electrical and mechanical domains of an electromechanical system, as is the case with the VEH system, the concept of load matching needs to be applied in the domain to which power is being delivered [14]. Figure 6 shows the circuit equivalent of the system represented by the bond graph in Fig. 5. It depicts the result of reflecting the mechanical flow source and the mechanical components across the gyrator. The obtained circuit allows direct application of the maximum power transfer theorem (MPTT) to determine the ideal Z_{load} . MPTT states that for a given power source with a known complex impedance, the maximum amount of power will be transferred to the attached load if the latter's complex impedance is equal to the complex conjugate of the impedance of the power source. In equation form, MPTT is simply:

$$Z_{load} = Z_{source}^* \quad (7)$$

where Z_{load} and Z_{source} are the complex impedances of the load and source respectively. Equation (7) states that the resistive component of the load's impedance will have the same magnitude as the resistive component of the source impedance; the reactive part of the load impedance, on the other hand, needs to be equal to the negative of the reactive part of the impedance of the source.

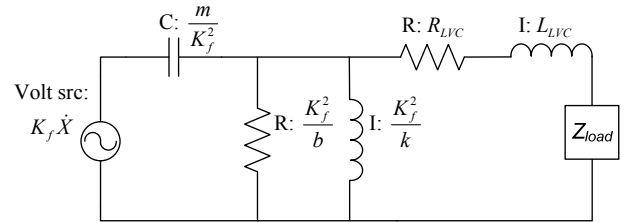


FIGURE 6. ELECTRICAL DOMAIN EQUIVALENT OF ENERGY HARVESTER

For conventional passive VEHs, Eq. (7) is applied only in part. Specifically, the resistive component of the load's impedance is matched to that of the source impedance. However, since the requirement on the load's reactance cannot be achieved passively, Eq. (7) is usually not applied to it. This results in passive harvesting behavior shown in Fig. 2, where maximum power generation occurs only at the harvester's natural frequency (Note: depending on the magnitude of the system's parasitic damping ratio, maximum power generation can occur at a frequency slightly different from the natural. However, as parasitic damping ratios are usually kept to a minimum in VEH design, the frequency at which it occurs is usually quite close to the natural frequency).

To facilitate the application of the MPTT to the experimental setup VEH, the harvester's electrical circuit equivalent from Fig. 6 was transformed into its Thévenin equivalent form.

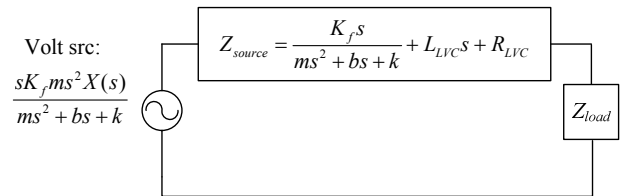


FIGURE 7. THÉVENIN EQUIVALENT CIRCUIT REPRESENTATION OF THE VEH

Figure 7 depicts the Thévenin equivalent circuit represented in the s-domain. In order to achieve maximum power generation passively, it is necessary to eliminate the reactive component of the combined system impedance and double its resistive component, without incorporating active elements in Z_{load} .

The frequency dependent behavior of Z_{source} is described by Eq. (8). This formulation imposes a requirement on the excitation frequency driving the VEH, a requirement which stems from the need to eliminate the reactive component, which can't be done by the purely resistive Z_{load} .

$$Z_{source} \Big|_{s=j\omega} = \left[R_{LVC} + \frac{K_f^2 b \omega^2}{(k - m\omega^2)^2 + (b\omega)^2} \right] + j \left[L_{LVC} \omega + \frac{K_f^2 \omega (k - m\omega^2)}{(k - m\omega^2)^2 + (b\omega)^2} \right] \quad (8)$$

Mathematically, this means that the j term of Eq. (8) needs to equal 0.

The harvester parameters used in determining the frequency of excitation which would yield maximum power transfer are shown in Table 1.

TABLE 1. VEH PARAMETERS

Parameter	Value
m	0.52 kg
b	6.8 N/(m/s)
k	1847 (N/m)
K_f	17.8 (N/A) or (V/(m/s))
L_{LVC}	0.0031 H
R_{LVC}	7 Ohms

The electrical parameter values were taken from the data sheet for the chosen LVC (BEI Kimco LA17-28-000A), except for R_{LVC} , which was increased slightly after directly measuring it. The mechanical parameters were obtained by the combination of measuring them (determining spring stiffness and estimating magnitude of proof mass) and observing the dynamic response of the mechanical system (curve fitting to determine damping and getting a better estimate of the proof mass). The dynamic response of the mechanical system alone was obtained by connecting a Kepco BOP 36-6 servo amplifier across the VEH leads and using the LVC as solely as a motor. The behavior that was expected is that of Eq. (9), where a force $K_f I(s)$ created by the Kepco generated current affects the relative position $P(s)$ of the proof mass, resulting in a mass-spring-damper system type of response.

$$\frac{P(s)}{K_f I(s)} = \frac{1}{ms^2 + bs + k} \quad (9)$$

The predicted model response and empirical data are shown to be in good agreement in Fig. 8.

Substituting the known magnitudes of all of the VEH components into Eq. (8) allows solving for the frequency at which the reactive j term becomes 0 as shown in Eq. (10).

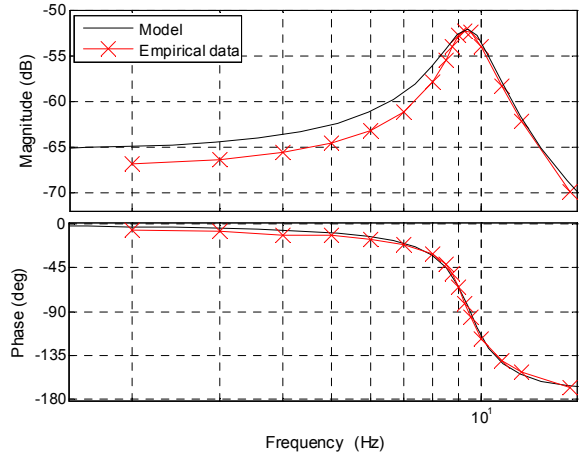


FIGURE 8. RESULTS OF MODELING m , b AND k HARVESTER PARAMETERS

Note that in solving for this frequency, the value used for physical viscous damping b was set to 6.2 N/(m/s) as opposed to 6.8 N/(m/s) which is stated in Table 1. This is due to slight physical changes in the experimental setup associated with its disassembly and reassembly between tests. The 6.8 N/(m/s) is the more current of the two values and will be used in future work unless noted otherwise.

$$\left[L_{LVC} \omega + \frac{K_f^2 \omega (k - m\omega^2)}{(k - m\omega^2)^2 + (b\omega)^2} \right] \Bigg|_{\substack{L_{LVC}=0.0031 \\ K_f=17.8 \\ k=1847 \\ m=0.52 \\ b=6.2}} = 0 \quad (10)$$

The condition shown in Eq. (10) is satisfied at two positive frequencies, $\omega_1 = 59.62$ rads/s and $\omega_2 = 447.17$ rads/s, corresponding to $f_1 = 9.49$ Hz and $f_2 = 71.17$ Hz respectively. Since f_2 is outside of the frequency range of interest (3-12 Hz), it was discarded. Substituting the obtained $\omega_1 = 59.62$ into Eq. 8 yields the VEH's equivalent internal electrical resistance at that particular frequency and the value to which the load resistance should be set in order to satisfy the MPTT passively, allowing maximum power generation at the excitation frequency of 9.49 Hz.

$$Z_{source} = \left[R_{LVC} + \frac{K_f^2 b \omega^2}{(k - m\omega^2)^2 + (b\omega)^2} \right] \Bigg|_{\substack{R_{LVC}=7 \\ K_f=17.8 \\ b=6.2 \\ \omega=59.62 \\ k=1847 \\ m=0.52}} = 58.10 \text{ Ohms}$$

$$Z_{load} = 58.10 \text{ Ohms}$$

The effect of attaching a load with the above equivalent resistance across the leads to the harvester's LVC can be modeled by assuming Z_{load} to simply be a 58.10 Ohm resistor and using Eqns. (5) and (6) to eliminate \mathbf{I} . The result can be used to solve for the frequency dependent relationship between the relative motion of the harvester's proof mass P and the acceleration of the excitation \ddot{X} . This relationship, when carried into the s-domain, is described by the transfer function shown in Eq. (12)

$$\frac{P(s)}{s^2 X(s)} = \frac{m(L_{LVC}s + R_{tot})}{L_{LVC}ms^3 + (mR_{tot} + bL_{LVC})s^2 + (bR_{tot} + kL + K_f^2)s + kR_{tot}} \quad (12)$$

where $R_{tot} = R_{LVC} + Z_{load}$, which is the total resistance of the VEH in the electrical domain. The relative accuracy of the above transfer function is depicted in Fig. 9. The solid line represents Eq. (12) with the VEH parameters from Tab. 1 and the solved for Z_{load} from Eq. (11) substituted in. The empirical data is collected from running the VEH with a 58.10 Ohm resistor connected across the LVC leads. The dashed line in Fig. 9 represents the ideal response of the system if maximum power transfer to the attached load was not frequency dependent, it is equivalent to the desired behavior that was shown in Fig. 2, and is discussed in detail in the next section.

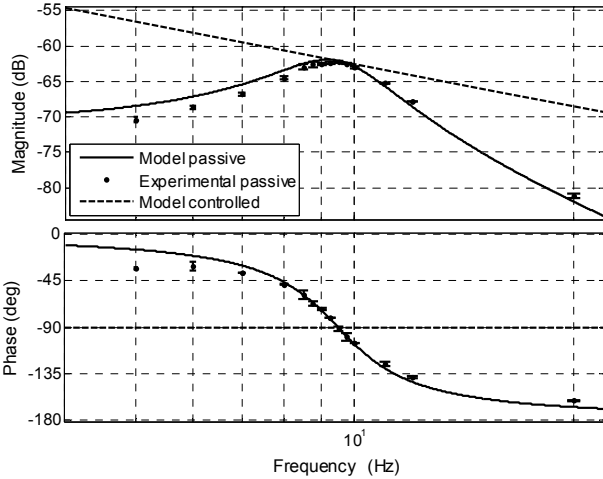


FIGURE 9. HARVESTER PROOF MASS DISPLACEMENT AMPLITUDE IN RESPONSE TO EXCITATION AT DIFFERENT FREQUENCIES

Active Electromagnetic Vibration Energy Harvesting

The previous section showed how to passively maximize energy harvesting by using the maximum power transfer theorem for load matching. Equation (8) showed that the VEH's internal impedance contains a reactive component which needed to be cancelled in accordance with the MPTT. Unfortunately, from observing the form of the source impedance in Fig. 7, it is evident

that no combination of passive components can be incorporated into Z_{load} in order to obtain an overall reactance of 0. Therefore, it was necessary to rely on a particular frequency to achieve the desired cancellation.

However, the MPTT required ideal load can be pursued actively, i.e., Z_{load} is made to be an actively varying impedance, that can exhibit specified dissipative (resistive) and conservative (reactive) behaviors. The control law that forces the load to behave in accordance with the MPTT removes the effect of frequency-dependent components, but leaves the same resistive behavior as that which was solved for in Eq. (11). This yields frequency independent maximum power generation. This MPTT dictated relationship is shown in Eq. (13) as a transfer function between the excitation acceleration and the proof mass relative position.

$$\frac{P_d(s)}{s^2 X(s)} = \frac{m(2R_{LVC} + \frac{K_f^2}{b})}{2(R_{LVC}b + K_f^2)s} \quad (13)$$

This transfer function was used to plot the dashed line representing the ideal behavior in Fig. 9. The ideal behavior defined by Eq. (13) can be further confirmed by plotting it on the same plot (Fig. 10) along with responses of several other theoretical passive harvesters with different spring stiffnesses (i.e., different natural frequencies).

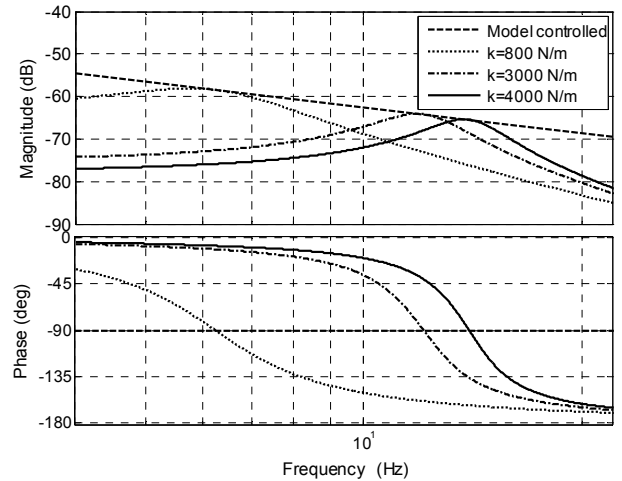


FIGURE 10. IDEAL BEHAVIOR DEFINED BY EQ. 13 COMPARED TO SEVERAL DIFFERENT PASSIVE HARVESTERS WITH DIFFERENT EQUIVALENT STIFFNESSES

The control law for obtaining this desired response described by Eq. (13) was derived by rewriting Eq. (5) with a control input U replacing the product of the motor constant and current yields, as shown below.

$$m\ddot{X} = m\ddot{P} + b\dot{P} + kP - U \quad (14)$$

$$ms^2 X(s) + U(s) = P(s)(ms^2 + bs + k)$$

In Eq. (14), the controller is assumed to drive the LVC to produce some force $U(s)$ upward, i.e., pushing the proof mass in the direction towards the bridge. Solving for which $U(s)$ will yield the relationship described by Eq. (13) yields:

$$U(s) = P(s)(ms^2 + (b(1 - 2R_{LVC}) - 2K_f^2)s + k) \dots - ms^2 X(s)(2R_{LVC} + \frac{K_f^2}{b} - 1) \quad (15)$$

The resulting control law shown in Eq. (15) is termed the Active Maximum Power Transfer (AMPT) controller.

Figure 11 shows simulation results in the form of normalized net average generated power of the passive VEH and that of the same VEH being governed by an AMPT controller. In simulation, the harvesters were subjected to four different excitation conditions ; these conditions are listed in Table 2 along with the reasons as to why they were chosen.

In simulation, net power was calculated based on the assumption that the LVC can behave as a 100% efficient generator. Although high efficiency regenerative electronics are not uncommon, the results should be treated as an upper bound on the performance of the controller. As discussed later in the Conclusion section, testing is being prepared to assess the capabilities of AMPT control experimentally.

TABLE 2. EXCTIATIONS USED IN SIMULATION

Excit. #.	Excitation Equation [mm] and Rationale for Choosing
1	$X(t) = 0.25 \sin(9.49 \cdot 2\pi t)$ Purpose: Comparison between passive and AMPT at frequency to which passive is tuned
2	$X(t) = 0.25 \sin(6 \cdot 2\pi t)$ Purpose: Comparison between passive and AMPT at frequency several Hz lower than that to which passive is tuned
3	$X(t) = 0.25 \sin(12 \cdot 2\pi t)$ Purpose: Comparison between passive and AMPT at frequency several Hz higher than that to which passive is tuned
4	$X(t) = 0.25 \sin(8 \cdot 2\pi t) + 0.15 \sin(13 \cdot 2\pi t) + \dots + 0.2 \sin(6 \cdot 2\pi t)$ Purpose: Comparison between passive and AMPT for excitations containing multiple frequency components

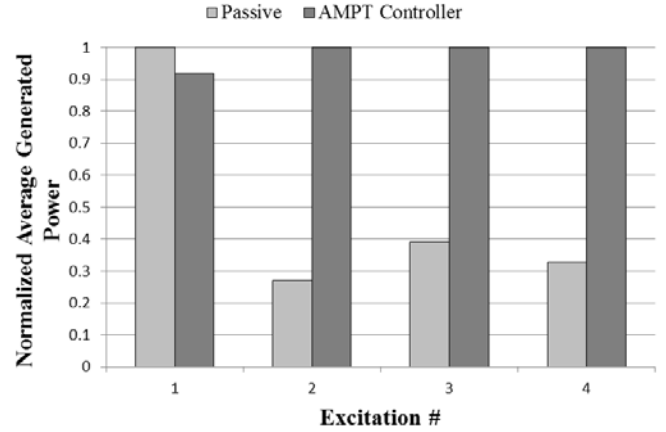


FIGURE 11. SIMULATION RESULTS OF PASSIVE AND AMPT ENERGY HARVESTING

From the results shown in Fig. 11, the distinct advantage the AMPT controlled VEH has over its passively operating counterpart is quite clear. The passive harvester does generate approximately 8% more average power than the AMPT controlled VEH at its ideal operating frequency. This is due to observed control chatter in the simulation, which may be a numerical error since no control signal should exist at the harvester's ideal operating frequency. However, even if this passive harvester advantage is accepted as real, it does not compensate for the significantly better power generation performance of its AMPT controlled counterpart for each other excitation mode used. Active harvesting generates approximately two to four times more power than passive at frequencies 2.5 Hz higher or lower than the latter's ideal. In addition, the AMPT controlled VEH showed roughly three times greater energy generation in the case where multiple frequency components were present in the excitation.

CONCLUSION

The presented research discussed the weakness of passive electromagnetic vibrational energy harvesting in applications where the harvester is not excited by one specific known frequency. An approach aimed at addressing this problem involving using the harvester as both a generator and a motor was presented. Design and modeling consideration, as well as conventional tuning of a passive vibrational energy harvester were discussed to further understand the problem. An experimental setup was constructed and utilized to experimentally verify the analyses and inferences drawn about passive energy harvesting. The conventional method for tuning passive harvesters, based on the maximum power transfer theorem, was used to derive a unique control law which makes use of the harvester as a motor to enforce maximum power transfer over a frequency range. This approach has a distinct advantage over the

traditional passive methodology, as it allows for a given harvester to be utilized in applications where the excitation frequency may change, or may contain several frequency components. The control law was verified in simulation, with initial data showing the control approach to have a distinct advantage in net power generation over conventional passive harvesting.

Immediate future work is aimed at determining the efficacy of the derived Active Maximum Power Transfer controller experimentally. Since active control requires transferring energy back and forth between the mechanical and electrical domains, the super capacitor bank shown in Fig. 3 will be used to determine whether the energy transport required by the AMPT controller can occur efficiently enough to generate a greater net amount of power than that which is generated in the passive case.

ACKNOWLEDGMENTS

This work was supported by NSF grant #1035627.

The authors would like to thank Mark E. Hofacker and Ozgur Yapar for their invaluable assistance on this project.

REFERENCES

- [1] T. Galchev, J. McCullagh, R. L. Peterson, K. Najafi, "Harvesting Traffic-Induced Bridge Vibrations," Conf. Rec. 2011 IEEE Transducers' 11, pp 5-9, June 2011.
- [2] U.S. Dept. of Transportation. "Our Nation's Highways: 2010" Web. <http://www.fhwa.dot.gov/policyinformation/pubs/hf/pl10023/fig7_3.cfm>.
- [3] O'Connell, Heather M.; Dexter, Robert J.; Bergson, Paul.; , "Fatigue Evaluation of the Deck Truss of Bridge 9340 - CTS Research Reports. "Center for Transportation Studies. University of Minnesota, 2007. Web.
- [4] Radio Broadcast. Minnesota Public Radio, Morning Edition. Jessica Mador. Sept. 16, 2008. 7:20 A.M.
- [5] J.P. Lynch, et al., "Design and performance validation of a wireless sensing unit for structural monitoring applications," *Structural Engineering and Mechanics*, vol 17, no. 3-4, 2004, pp. 393-408.
- [6] Pedchenko A.V., Hoke J. W., and Barth E. J. "A Control Approach for Broadening the Operating Frequency Range of a Bridge Vibration Energy Harvester," Paper accepted for 2011 Dynamic Systems and Control Conference, publication pending. Nov. 2011
- [7] Beeby, S. P., M. J. Tudor, and N. M. White. "Energy Harvesting Vibration Sources for Microsystems Applications," *Meas. Sci. Technol.* 17 (2006): 175-95. IOPscience. Web.
- [8] Williams, C. B., A. Pavic, R. S. Crouch, and R. C. Woods. "Feasibility study of vibration-electric generator for bridge vibration sensors," Vibration Engineering Research Section, University of Sheffield. Society for Experimental Mechanics. Web.
- [9] A. Shahabadi, (1977). Bridge Vibration Studies: Interim Report. Purdue e-Pubs [Online] pp. 108-130 Available:<http://docs.lib.purdue.edu/cgi/viewcontent.cgi?article=2303>
- [10] M. Wang, 2004. "Embedded Strain Sensor With Power Scavenging From Bridge Vibration," Master's Thesis. University of Maryland.
- [11] Sazonov, E.; Haodong Li; Curry, D.; Pillay, P.; "Self-Powered Sensors for Monitoring of Highway Bridges," *Sensors Journal*, IEEE, vol.9, no.11, pp.1422-1429, Nov. 2009
- [12] Y. Wang, et al., "Vibration Monitoring of the Voigt Bridge using Wired and Wireless Monitoring Systems," Proceeding of 4th China-Japan-US Symposium on Structural Control and Monitoring, Oct.16-17, 2006
- [13] M. Gioffrè et al., 2002. "Comparison between accelerometer and laser vibrometer to measure traffic excited vibrations on bridges," *Shock and Vibration*, 9(1), Feb, pp. 11-18.
- [14] N. G. Stephen., 2006. "On the maximum power transfer theorem within electromechanical system," *Journal of Mechanical Engineering Science*, Vol. 220. pp. 1261-1267